SCIENTIFIC REPORTS

OPEN

In situ solid-state fabrication of hybrid AgCl/AgI/AgIO$_3$ with improved UV-to-visible photocatalytic performance

Jing Xie, Yali Cao, Dianzeng Jia, Yizhao Li, Kun Wang & Hui Xu

The AgCl/AgI/AgIO$_3$ composites were synthesized through a one-pot room-temperature *in situ* solid-state approach with the feature of convenient and eco-friendly. The as-prepared composites exhibit superior photocatalytic performance than pure AgIO$_3$ for the degradation of methyl orange (MO) under both UV and visible light irradiation. The photodegradation rate toward MO of the AgCl/AgI/AgIO$_3$ photocatalyst can reach 100% after 12 min irradiation under UV light, or 85.4% after 50 min irradiation under visible light, being significantly higher than AgCl, AgI, AgIO$_3$ and AgI/AgIO$_3$. In addition, the AgCl/AgI/AgIO$_3$ photocatalyst possesses strong photooxidation ability for the degradation of rhodamine B (RhB), methylene blue (MB), phenol, bisphenol A (BPA) and tetracycline hydrochloride under visible light irradiation. The reactive species capture experiments confirmed that the h$^+$ and $\bullet$O^{2-} play an essential role during the photocatalytic process under UV light or visible light irradiation. The enhanced effect may be beneficial from the enhanced light adsorption in full spectrum and increased separation efficiency of photogenerated hole-electron pairs, which can be ascribed to the synergistic effect among AgCl, AgI and AgIO$_3$ nanoplates in AgCl/AgI/AgIO$_3$ composites.

Semiconductor photocatalytic oxidation technique has attracted widespread attention on the degradation of environmentally hazardous substances due to its potential utilization of solar energy, the high conversion rate of solar energy and the strong oxidation ability[1,2]. In recent years, nanoscaled TiO$_2$ have been regarded as one of most promising materials in photocatalytic field because of its high photocatalytic activity, stability and non-poisonous[3–5]. Nevertheless, TiO$_2$ has a wide band gap of 3.2 eV which lead to low quantum yields as well as the lack utilization of visible light (the main component of solar spectrum)[6,7]. Therefore, photocatalyst with full-spectrum catalysis ability are highly desired for environmental purification.

Recently, a growing number of Ag-based oxy-acid salts photocatalysts, such as Ag$_3$PO$_4$[8], Ag$_3$VO$_4$[9], Ag$_2$WO$_4$[10], Ag$_2$CO$_3$[11] and AgIO$_3$[12] have exhibited novel catalysis efficiency on the degradation of environmental hazardous. Among them, AgIO$_3$ has aroused a great deal attention in photocatalytic field due to the lone pair electrons of I^{5+} is beneficial to form layered structure in crystal[13]. Unfortunately, just like TiO$_2$, the band gap of AgIO$_3$ was empirically calculated to be 3.38 eV, leading to its sluggish reaction to visible light[14]. To date, composite photocatalysts have been proved to be a feasible strategy to overcome the drawbacks via the so-called synergetic effects. To optimize the photocatalytic performance of AgIO$_3$, researchers have attempted to couple AgIO$_3$ with other Ag-based materials to upgrade its response to visible light and inhibit the recombination of electron-holes[15,16]. For instance, He *et al.* has reported that Ag/AgIO$_3$ composites were fabricated by the combination of the solid-state and liquid phase method, it displayed high photocatalytic activity in the conversion of CO$_2$ to CH$_4$ and CO under visible light irradiation[17]. Zeng *et al.* prepared Ag/AgI/AgIO$_3$ by a hydrolysis method and followed an *in-situ* reduction reaction, the composites also exhibited better photocatalytic performance than pure AgIO$_3$ under both UV light and visible light irradiation[18]. Despite a few successful examples have convinced that composite structures can improve the photocatalytic activity of pure AgIO$_3$, the multiple-steps operations for preparing Ag-based composites continuously limit their large scale application due to the complicated procedures that caused time and

Key Laboratory of Energy Materials Chemistry, Ministry of Education, Key Laboratory of Advanced Functional Materials, Autonomous Region, Institute of Applied Chemistry, Xinjiang University, Urumqi, 830046, Xinjiang, P.R. China. Correspondence and requests for materials should be addressed to Y.C. (email: caoyali523@163.com) or D.J. (email: jdz@xju.edu.cn)
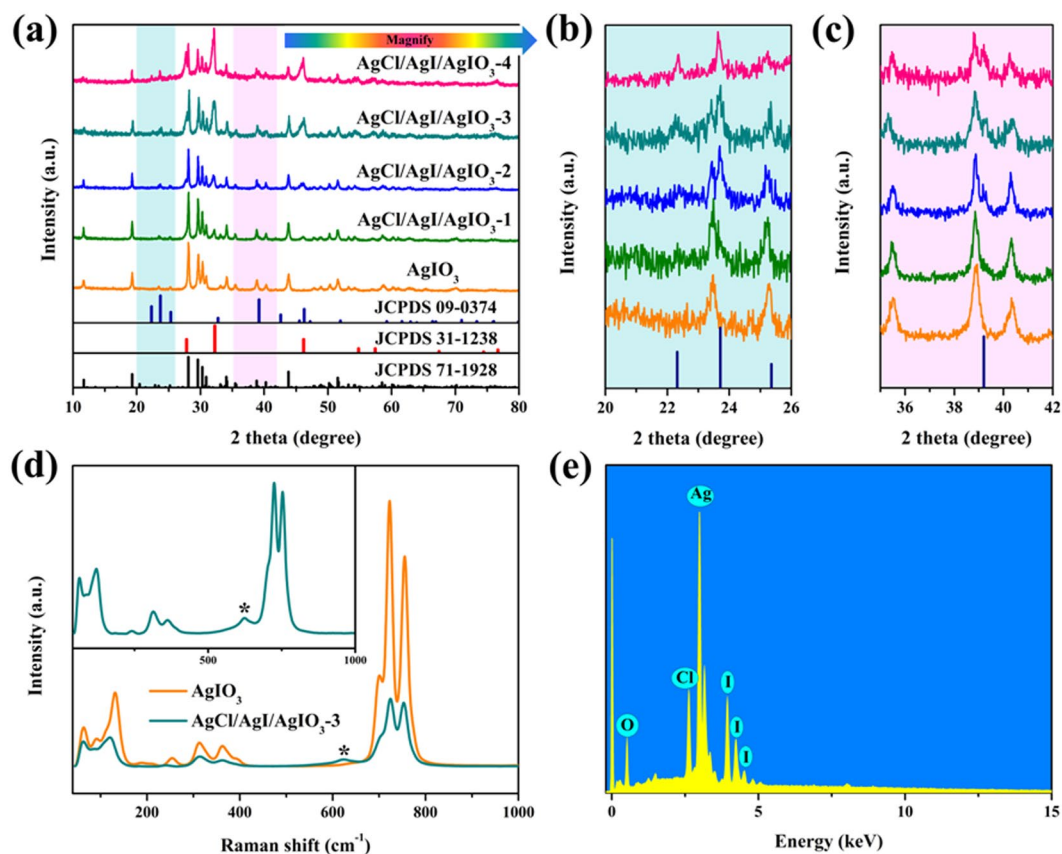
Figure 1. XRD patterns (**a–c**) and Raman spectrum (**d**) of the pure AgIO$_3$ and AgCl/AgI/AgIO$_3$ composites, (**e**) EDS of the AgCl/AgI/AgIO$_3$ composites.

energy consumption. Thus, it is necessary to develop a simple and efficient approach for rationally fabricating Ag-based composites.

Herein, the AgCl/AgI/AgIO$_3$ composites was designed and synthesized by a one-pot solid-state technique utilizing AgIO$_3$ as a self-sacrificing template and HONH$_3$Cl as reducing agent. This method has the feature of simplicity, rapidity, low cost and high yield[19–21]. The photocatalytic performance of the AgCl/AgI/AgIO$_3$ composites was evaluated by the decomposition of various kinds of organic contaminants under visible light irradiation. Furthermore, the photocatalytic mechanisms of the AgCl/AgI/AgIO$_3$ composites correlating to different light source were also systematically investigated. This study may open up a promising approach to design and synthesize composite photocatalysts for environmental purification.

Results and Discussions

Figure 1a showed the XRD patterns of the as-prepared pure AgIO$_3$ and AgCl/AgI/AgIO$_3$ composites. As demonstrated in Fig. 1a, the diffraction peaks of pure AgIO$_3$ at 2θ values of 11.60°, 19.29°, 28.09°, 29.65°, 30.30°, 30.91°, 34.11°, 38.87°, 43.86° and 51.5° were assigned to (020), (021), (041), (211), (230), (002), (231), (001), (232) and (271) crystal planes of the orthorhombic AgIO$_3$ (JCPDS 71-1928), respectively. No impurity peaks were found, indicating the high purity of the pure AgIO$_3$. In AgCl/AgI/AgIO$_3$ composites, peaks located at 2θ = 27.80°, 32.16° and 46.18° were appeared, which match well with (111), (200) and (220) planes of cubic AgCl (JCPDS 31-1238), respectively. Besides, as observed in the enlarged XRD patterns (Fig. 1b and c), two small peaks situated at 2θ values of 23.70° and 39.20° were attributed to (002) and (110) planes of AgI (JCPDS 09-0374), respectively. Furthermore, with the increase of the amount of reductant, the characteristic peaks of AgIO$_3$ decreased in intensity gradually, while the characteristic peaks of AgCl and AgI increased in intensity simultaneously, which verifies the conversion from AgIO$_3$ to AgCl and AgI through the solid-state reaction between AgIO$_3$ and HONH$_3$Cl. However, the position of the diffraction peaks belong to AgIO$_3$ did not shift in AgCl/AgI/AgIO$_3$ composites, which suggested that the crystal phase structure of AgIO$_3$ did not change after the introducing of AgCl and AgI. Moreover, the Raman spectrum of the pure AgIO$_3$ and AgCl/AgI/AgIO$_3$-3 (Fig. 1d) were tested, it was clearly seen that the Raman bands of the samples are almost the same, whereas the intensity of AgCl/AgI/AgIO$_3$-3 is significantly decreased compared to pure AgIO$_3$, which further illustrated that the *in situ* solid-state reaction occurred between AgIO$_3$ and HONH$_3$Cl. A new characteristic peak appears at 623.5 cm^{-1}, which can be ascribed to the vibration peak of AgCl[22,23], the result is coincident with the result of XRD. To further identify the component elements of AgCl/AgI/AgIO$_3$ composites, the EDS of the AgCl/AgI/AgIO$_3$-3 were performed. As depicted in Fig. 1e, it also confirmed the coexistence of Ag, O, Cl and I in the AgCl/AgI/AgIO$_3$-3 composites.
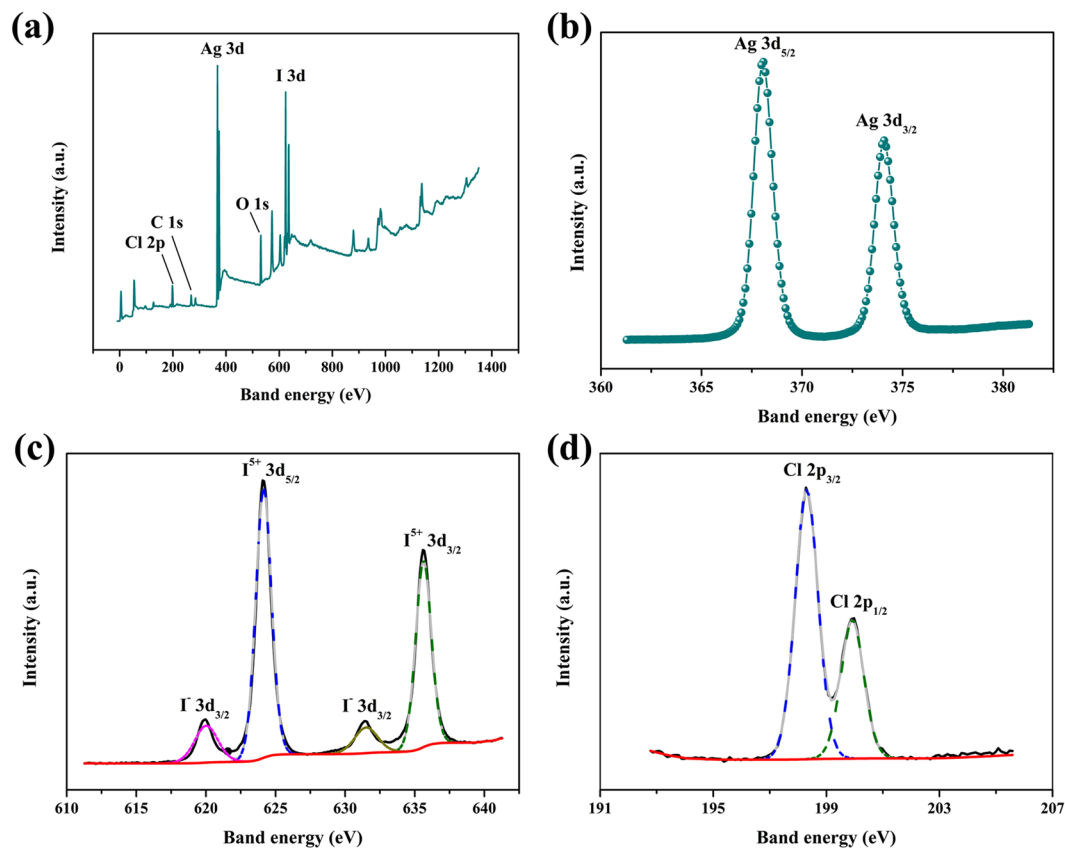
Figure 2. XPS spectra of the AgCl/AgI/AgIO$_3$-3: (**a**) survey scan, (**b**) Ag 3d, (**c**) I 3d, (**d**) Cl 2p.

To provide direct evidence for confirming the surface chemical composition and the chemical states of the as-prepared samples, the XPS full-scan spectrum was employed. Wherein only the Ag 3d, O 1 s, I 3d, Cl 2p and a trace of C 1 s species were detected (Fig. 2a). The corresponding high-resolution XPS spectra in Fig. 2b–d display the characteristic peaks of Ag 3d, I 3d and Cl 2p over the AgCl/AgI/AgIO$_3$-3 sample. Peaks with binding energies of 368.08 eV and 374.08 eV are associated with Ag$^+$ 3d$_{5/2}$ and Ag$^+$ 3d$_{3/2}$ peaks, respectively (Fig. 2b). Two peaks at 624.08 eV and 635.58 eV can be ascribed to I^{5+} 3d$_{5/2}$ and I^{5+} 3d$_{3/2}$, and meantime the peaks at 619.98 eV and 631.48 eV match the features of I$^-$ 3d$_{5/2}$ and I$^-$ 3d$_{3/2}$, respectively (Fig. 2c). This result demonstrates the co-existence of I^{5+} and I$^-$. As shown in Fig. 2d, the peaks at 198.28 and 199.98 eV in AgCl/AgI/AgIO$_3$-3 are detected, which can be ascribed to Cl 2p$_{3/2}$ and Cl 2p$_{1/2}$. The XPS results confirmed the three substances (AgCl, AgI and AgIO$_3$) exist simultaneously in the AgCl/AgI/AgIO$_3$-3 sample, further illustrating the formation of the composites.

To investigate the morphology evolution of various samples, the FESEM imaging was measured. As displayed in Fig. 3a, the pure AgIO$_3$ is major composed of nanosheets with smooth surfaces, and the sizes of these nanosheets are approximately 2~4μm × 500~600 nm (length × wide). However, the sizes of the nanosheets become smaller and a certain amount of irregular nanoparticles are distributed on the surface and vicinity of AgIO$_3$ nanosheets after the introduction of the reducing agent, illustrating that the formation of AgCl and AgI. With increasing amount of HONH$_3$Cl, the sizes of the AgIO$_3$ nanosheets become smaller, meanwhile, more AgCl and AgI nanoparticles generate. Figure 3(b–e) clearly shows the morphology evolutions from AgIO$_3$ nanosheets to Ag-AgI-AgIO$_3$ composites with irregular nanoparticles. EDS mapping was employed to further identify the elemental composition and distribution of pure AgIO$_3$ and AgCl/AgI/AgIO$_3$-3. Supplementary Fig. S1 reveals that Ag, O and I elements exist in pure AgIO$_3$ and all of them were uniformly distributed in AgIO$_3$. After reduced by HONH$_3$Cl, Cl element was introduced into this system and with the other three elements (Ag, O and I) well-distributed in AgCl/AgI/AgIO$_3$-3 (Fig. 3f–i), once again illustrating that the AgCl and AgI was well distributed on the AgIO$_3$.

TEM was also employed to investigate the morphology of the pure AgIO$_3$ and AgCl/AgI/AgIO$_3$-3. As shown in Fig. 3j, pure AgIO$_3$ was composed of regular rectangular nanosheets with 4μm in length and 600 nm in width. However, the shape of the perfect nanosheets was destroyed after the accretion of reductant, as displayed in Fig. 3k. The sizes of the nanosheets decreased, in addition, there are a certain amount of substances with irregular morphologies appeared on the surface or the edge of the nanosheets. This phenomenon also can be observed in others regions of the sample, as seen in the low-magnification TEM (Supplementary Fig. S2), which is consistent with the SEM result.

To the best of our knowledge, composite structures are generally obtained through several multiple-step approaches that include *in situ* reduction reaction, photoreduction and ion-exchange reaction in solutions[24–26].
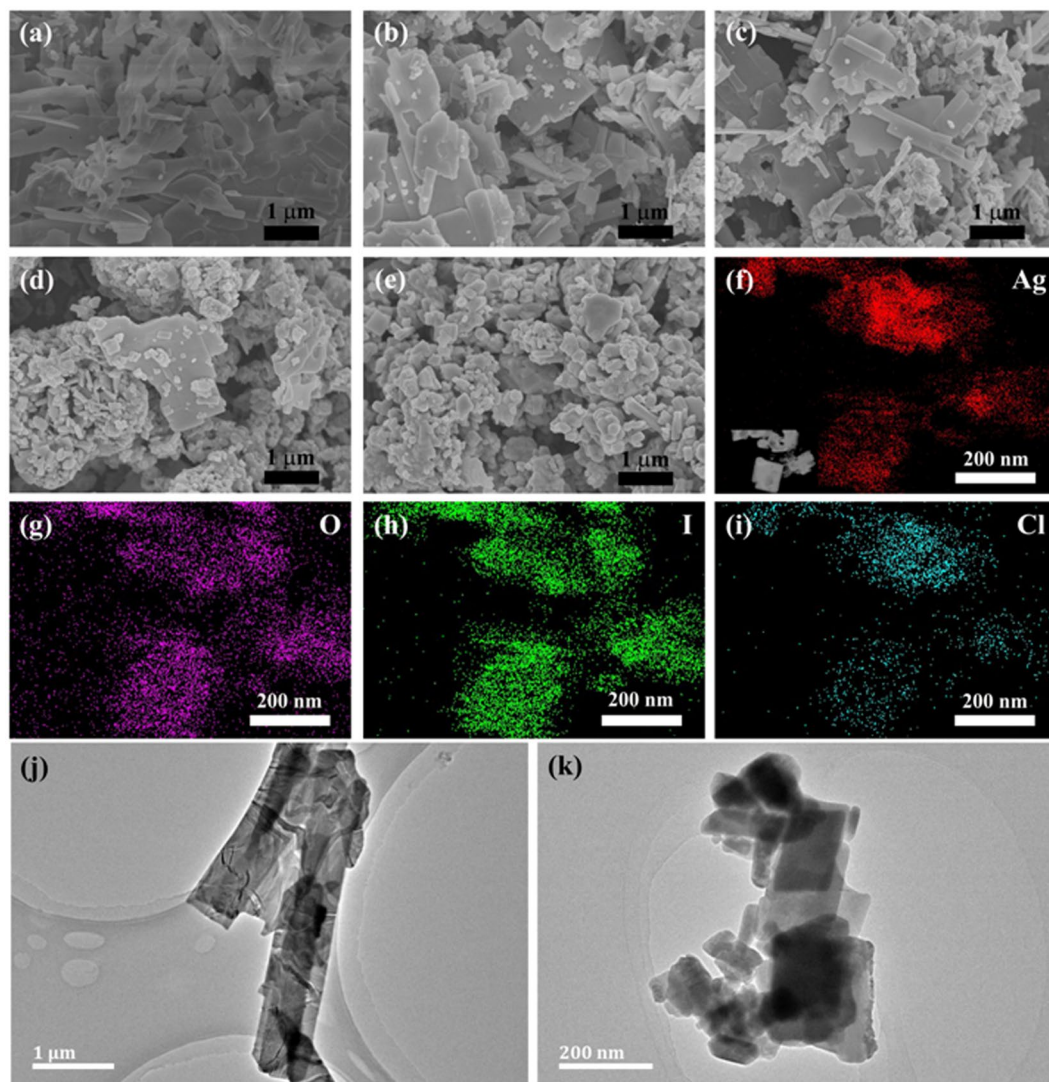
Figure 3. FESEM images of pure $AgIO_3$ (**a**), AgCl/AgI/$AgIO_3$-1 (**b**), AgCl/AgI/$AgIO_3$-2 (**c**), AgCl/AgI/$AgIO_3$-3 (**d**), and AgCl/AgI/$AgIO_3$-4 (**e**), respectively. EDS mapping of AgCl/AgI/$AgIO_3$-3 (**f–i**). TEM images of pure $AgIO_3$ (**j**) and AgCl/AgI/$AgIO_3$-3 (**k**), respectively.
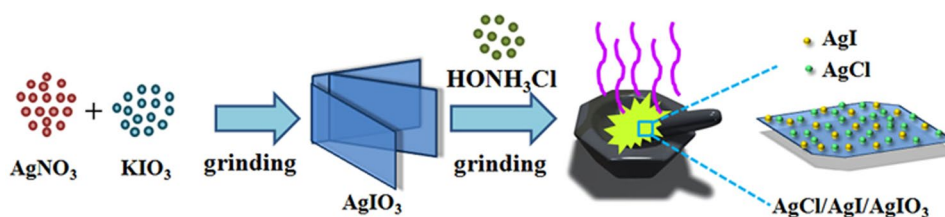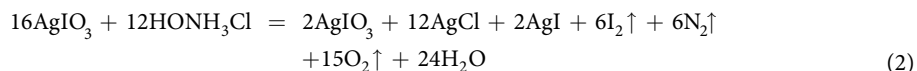

Figure 4. Schematic illustration of the possible formation process of the AgCl/AgI/$AgIO_3$ composites.

Although, these methods can obtain the materials with tailored properties by adjusting the reactive condition in each step, they are addicted to complicated process and time consumption. In this study, a simple and rapid one-pot *in situ* solid-state method was first applied to fabricate AgCl/AgI/$AgIO_3$ composites and the $AgIO_3$ nanosheets was employed as a self-sacrificing template. A schematic illustration of the possible formation process of the AgCl/AgI/$AgIO_3$ composites was shown in Fig. 4. Firstly, the $AgIO_3$ nanoplates were obtained by a metathesis reaction between $AgNO_3$ and KIO_3 powder at room temperature. The process accompanied with the release of heat and vapor, the moist powders were acquired after grinding 10 min and the $AgIO_3$ nanosheets produced. Subsequently, the prepared $AgIO_3$ was reacted with $HONH_3Cl$ by an *in situ* oxidation-reduction reaction in solid state. Interesting, the $HONH_3Cl$ plays a dual role in this process, which is not only as a reducing agent, but also

provides the chloride ion. When the $HONH_3Cl$ added into this reaction system, the purple gas comes out at once and the color of the product changes from white to yellow-green as soon as possible. Based on the above phenomena, the reaction that occurred in the formation of $AgCl/AgI/AgIO_3$ crystal nuclei may be explained by equations (1 and 2):

$$AgNO_3 + KIO_3 = AgIO_3 + KNO_3 \tag{1}$$

$$16AgIO_3 + 12HONH_3Cl = 2AgIO_3 + 12AgCl + 2AgI + 6I_2\uparrow + 6N_2\uparrow \\ +15O_2\uparrow + 24H_2O \tag{2}$$

Since $AgIO_3$ is a typical photocatalyst that only responded in the ultraviolet region, the photocatalytic activities of pure $AgIO_3$ and $AgCl/AgI/AgIO_3$ composites were first investigated through degrading MO aqueous solution under UV light irradiation. As displayed in Fig. 5a, all the $AgCl/AgI/AgIO_3$ composites possess better photocatalytic activity on the degradation of MO under UV light irradiation than pure $AgIO_3$. The apparent first-order rate constants of the as-prepared photocatalysts first increased gradually and then decreased along with increase in the amount of $HONH_3Cl$. The $AgCl/AgI/AgIO_3$-3 composites exhibited the best photocatalytic activity in all photocatalysts and it's apparent first-order rate constants is $18.91 \times 10^{-2}\,min^{-1}$, which is about 24.8 times of pure $AgIO_3$ ($0.76 \times 10^{-2}\,min^{-1}$). In Fig. 5b, the typically absorption peak of $AgCl/AgI/AgIO_3$-3 photocatalyst towards the MO is decreased dramatically with the increase of illumination time and the color of the dye become faded, until disappeared and colourless. The degradation of MO over the $AgCl/AgI/AgIO_3$-3 is 100% with the irradiation of UV light after 12 min. Since the sun light is mainly composed of ~5% ultraviolet light and 43% visible light, the exploration of photocatalysts which can make full use of sunlight is the primary task in this field[27,28]. Accordingly, the photocatalytic performances of the as-prepared photocatalysts were also investigated under visible light excitation. As seen in Fig. 5c, the trend of the photocatalytic oxidation of MO over all photocatalysts is basically consistent with the results with UV irradiation. The $AgCl/AgI/AgIO_3$-3 composites still shows the outstanding photooxidation ability towards MO and it's photodegradation rate constants is $3.69 \times 10^{-2}\,min^{-1}$, which is much higher than the pure $AgIO_3$ ($0.01 \times 10^{-2}\,min^{-1}$) and other $AgCl/AgI/AgIO_3$ composites as well. In Fig. 5d, the typically absorption peak of the MO over $AgCl/AgI/AgIO_3$-3 photocatalyst is also diminished rapidly and the color of the dye also become shallower as the increase of illumination time. It is calculated that the degradation of MO over the $AgCl/AgI/AgIO_3$-3 is 85.4% after 50 min irradiation of visible light. The photocatalytic activity of $AgCl/AgI/AgIO_3$-3 was better than the pure AgCl, AgI and $AgIO_3$ composite, as presented in Supplementary Figs S3 and S4, illustrating the important role of synergistic effect in $AgCl/AgI/AgIO_3$-3. In addition, the $AgCl/AgI/AgIO_3$-3 composite still reveals a better performance on the photocatalytic degradation of MO under both UV and visible light irradiation than the mechanical mixtures of AgCl, AgI and $AgIO_3$ (see Supplementary Fig. S5), which further indicated the importance of the *in situ* reaction to the synergistic effects.

In order to investigate the best excitation wavelength and the light absorption properties of $AgCl/AgI/AgIO_3$-3 composite, the wavelength dependent photocatalytic activity of $AgCl/AgI/AgIO_3$-3 was tested for the degradation of MO by a 300 W Xe with different band-pass filter (Supplementary Fig. S6). Besides, the wavelength dependent photocatalytic activities over $AgCl/AgI/AgIO_3$-3 were also calculated as apparent quantum yields[29,30], as displayed in Fig. 5e. The $AgCl/AgI/AgIO_3$-3 composite features excellent photooxidation ability for MO under all test wavelengths and shows high photocatalytic activity at 400 nm, suggesting that $AgCl/AgI/AgIO_3$-3 composites has a good photoresponse to the full-spectrum and also implying that 400 nm was the best excitation wavelength. In order to evaluate the repeatability and stability of the photocatalyst, the recycling experiment was conducted on the visible photocatalytic degradation of MO. Figure 5f shows that there is a little decrease after three consecutive cycles, which could attribute to the conversion of a part of I^{5+} to I^- (Supplementary Fig. S7). The reaction changed the relative contents of AgCl, AgI and $AgIO_3$, which is the disadvantage for recycling.

Different kinds of organic pollutants had been used to evaluate the photocatalytic performance of the $AgCl/AgI/AgIO_3$-3 composite comprehensively, besides cationic dye MO, anionic dye rhodamine B (RhB) and methylene blue (MB), neutral stubborn pollutants phenol, bisphenol A (BPA) and tetracycline hydrochloride. Figure 6a–e displays the typically absorption peak of RhB, MB, phenol, BPA and tetracycline hydrochloride, respectively, over $AgCl/AgI/AgIO_3$-3 photocatalyst with visible light. Surprisingly, the $AgCl/AgI/AgIO_3$-3 photocatalyst possesses the excellent degradation effects on all types of pollutants except for phenol. The low degrading efficiency of phenol may due to the P-π conjugative effect, which lead to the fracture of C-O bond is very difficult (Supplementary Fig. S9). The apparent first-order rate constants for the degradation of MO, RhB, MB, phenol, BPA and tetracycline hydrochloride over $AgCl/AgI/AgIO_3$-3 photocatalyst is $3.69 \times 10^{-2}\,min^{-1}$, $2.21 \times 10^{-2}\,min^{-1}$, $2.29 \times 10^{-2}\,min^{-1}$, $0.20 \times 10^{-2}\,min^{-1}$, $0.80 \times 10^{-2}\,min^{-1}$ and $1.47 \times 10^{-2}\,min^{-1}$, respectively (Fig. 6f), illustrating the $AgCl/AgI/AgIO_3$-3 photocatalyst almost can degrade various kinds of organic pollutants effectively.

Composites are always considered as effective means to improve photocatalytic activity owing to the tunable band structures and efficient electron-hole separation and transportation[31,32]. The UV-vis diffuse reflectance spectroscopy was employed to study the light absorbance property of the as-synthesized samples. As revealed in Fig. 7a, the absorption threshold of pure $AgIO_3$ is situated at about 350 nm and the band gap energy of pure $AgIO_3$ (3.8 eV) was calculated through the Tauc plot extrapolation (see Supplementary Fig. S10), indicating that the pure $AgIO_3$ is unresponsive to visible light. While the as-prepared $AgCl/AgI/AgIO_3$ composites exhibit enhanced adsorption in full spectrum with the increase amount of $HONH_3Cl$, especially the absorption range at 300–420 nm and 450–800 nm, which should be assigned to the generation of AgCl and AgI on the surface of $AgIO_3$. Particularly, the $AgCl/AgI/AgIO_3$-3 sample exhibits the supreme absorption among all the samples, implying the best photocatalytic activity. In addition, the color of the as-prepared samples changes from white to light-green,
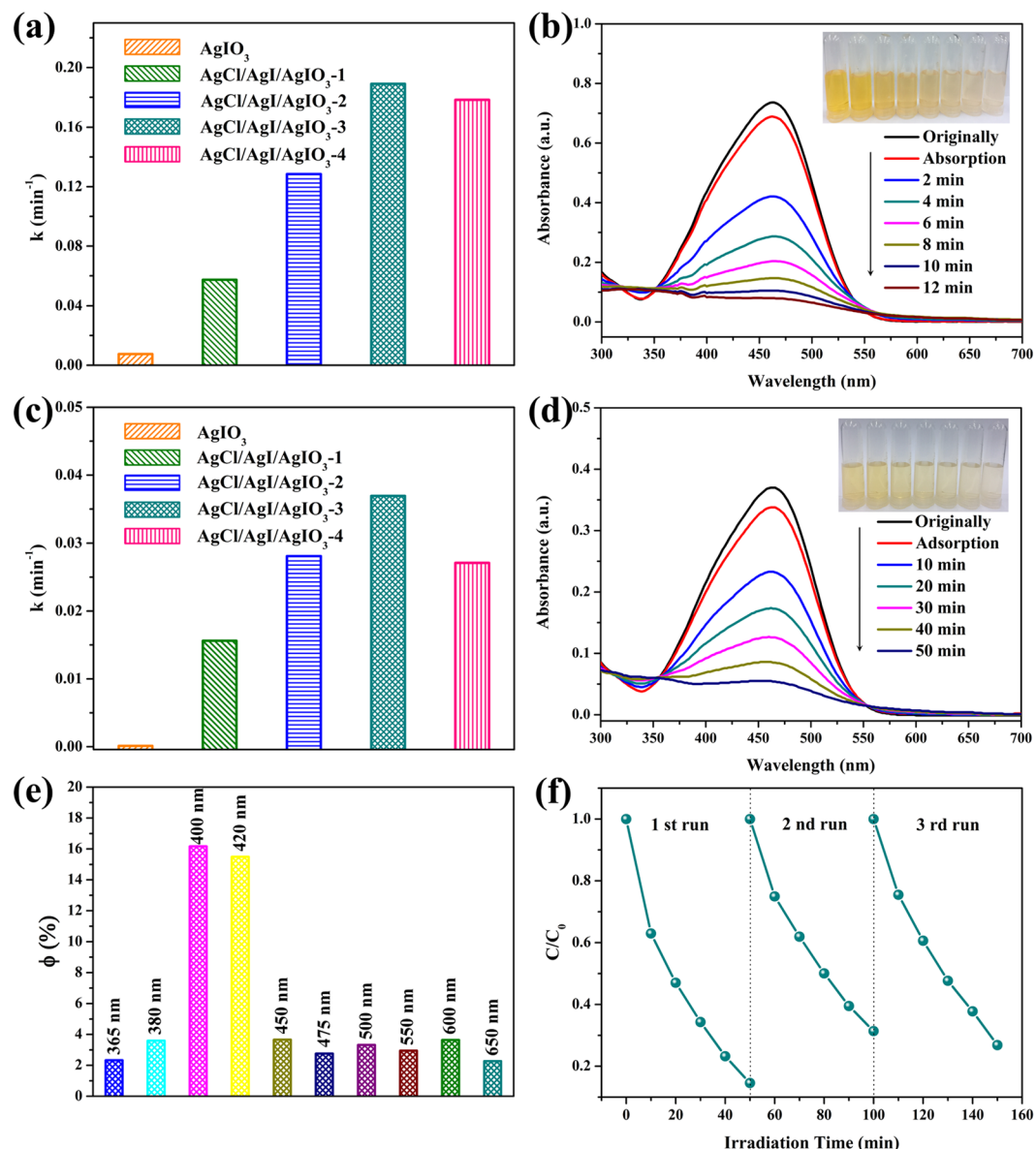
Figure 5. (**a**) The apparent first-order rate constants of photocatalytic degradation of MO over $AgIO_3$ and $AgCl/AgI/AgIO_3$ composites under UV light irradiation, (**b**) temporal UV-vis spectral change of MO with irradiation time over $AgCl/AgI/AgIO_3$-3 under UV light irradiation, (**c**) the apparent first-order rate constants of photocatalytic degradation of MO over $AgIO_3$ and $AgCl/AgI/AgIO_3$ composites under visible light irradiation, (**d**) temporal UV-vis spectral change of MO with irradiation time over $AgCl/AgI/AgIO_3$-3 under visible light irradiation, (**e**) the calculated apparent quantum yields over the $AgCl/AgI/AgIO_3$-3 composite depended on wavelength, (**f**) recycling experiments were conducted on the visible photocatalytic degradation of MO by $AgCl/AgI/AgIO_3$-3 composites.

and finally to yellow-green (the insert of Fig. 7a), suggesting that the orderly enhanced response to visible light with the increase in the amount of $HONH_3Cl$. Based on the above analysis, the light absorption can be effectively strengthened by the collaborative effects of AgCl, AgI and $AgIO_3$.

Subsequently, the photoluminescence (PL) spectrum was employed to appraise the charge separation of electron-hole pairs[33]. As shown in Fig. 7b, all the $AgCl/AgI/AgIO_3$ composites demonstrate significant decrease of the photoluminescence emission intensity as compared to pure $AgIO_3$, and the intensity gradually decreased with the increase of $HONH_3Cl$, illustrating that the $AgCl/AgI/AgIO_3$ composites can effectively hinder the recombination of electron-hole pairs and the amount of $HONH_3Cl$ can optimize the phtocatalytic activity of $AgIO_3$. The $AgCl/AgI/AgIO_3$-3 sample also reveals the lowest intensity of photoluminescence emission, suggesting that $AgCl/AgI/AgIO_3$-3 has the best electron-hole separation property. Time resolved photoluminescence spectra of pure $AgIO_3$ and $AgCl/AgI/AgIO_3$-3 composite also indicated more non-radiative transfer of photogenerated charge carriers in $AgCl/AgI/AgIO_3$-3 composite (Supplementary Fig. S11).
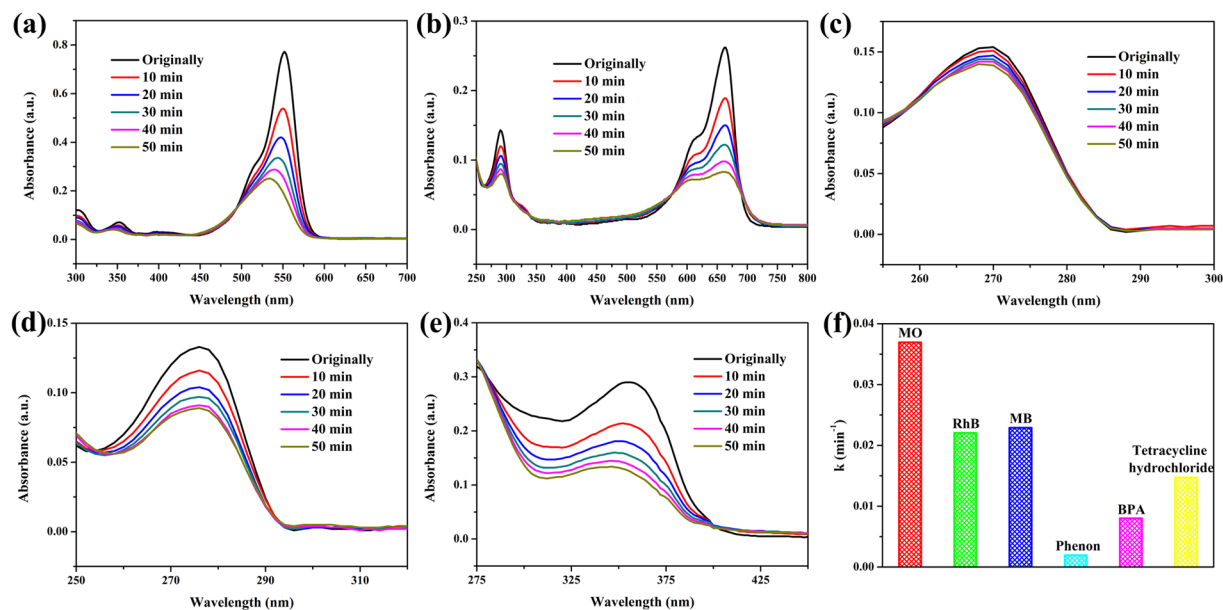
Figure 6. Temporal UV-vis spectral change of RhB (**a**), MB (**b**), phenol (**c**), BPA (**d**) and tetracycline hydrochloride (**e**) with irradiation time over AgCl/AgI/AgIO$_3$-3 composite, (**f**) the apparent first-order rate constants of photocatalytic degradation of MO, RhB, MB, phenol, BPA and tetracycline hydrochloride over AgCl/AgI/AgIO$_3$-3 composite under visible light irradiation.
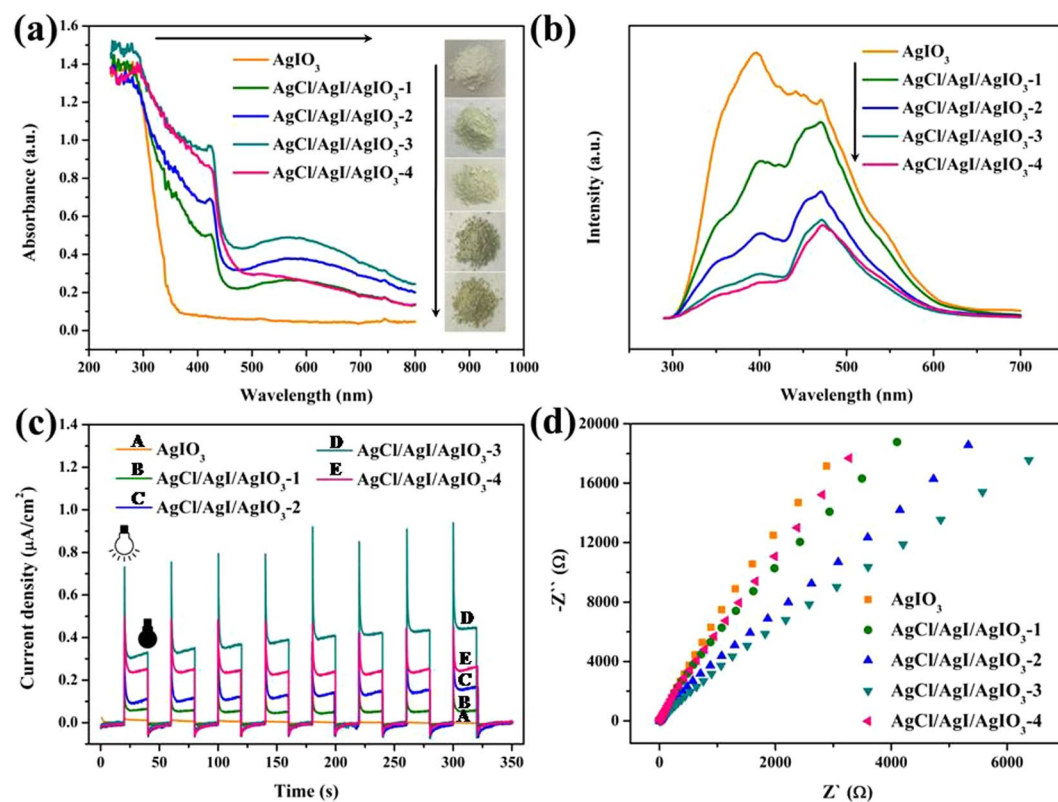

Figure 7. UV-vis diffuse reflectance spectroscopy and photograph (**a**), fluorescence spectrum with 280 nm excitation wavelength (**b**), photocurrent density with visible light irradiation (**c**) and EIS Nyquist plots (**d**) of pure AgIO$_3$ and AgCl/AgI/AgIO$_3$ composites.
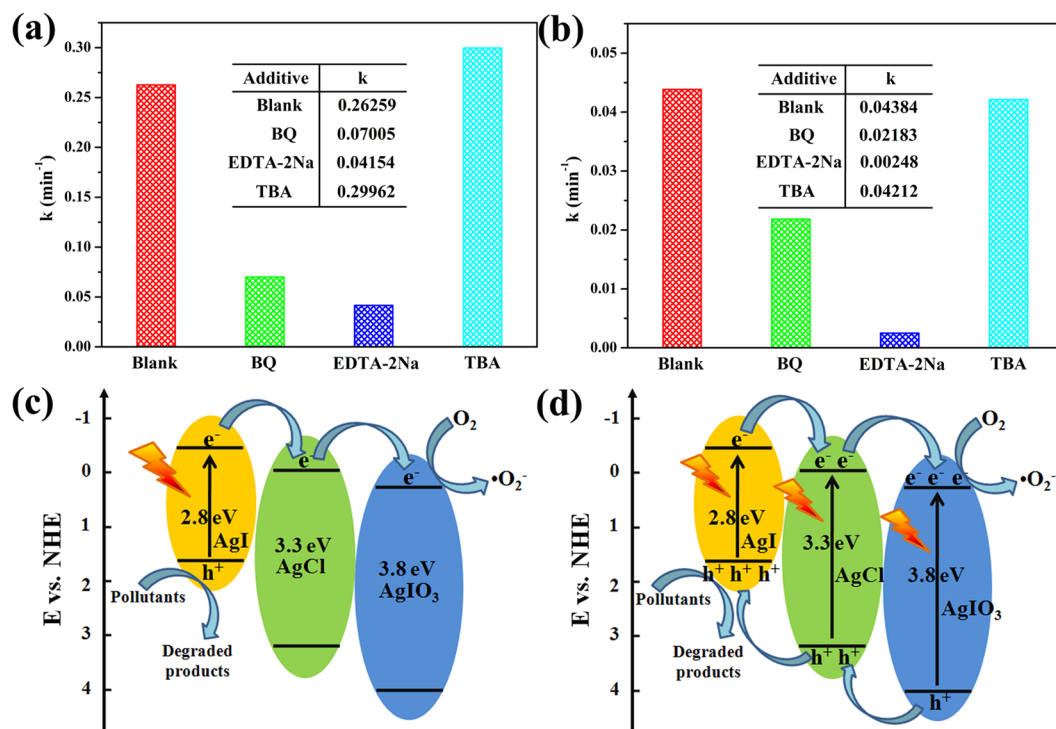
Figure 8. The plots of photogenerated charges trapping experiment on the photocatalytic degradation of MO over AgCl/AgI/AgIO$_3$-3 composites under UV light (**a**) or visible light irradiation (**b**), photocatalytic mechanism process of AgCl/AgI/AgIO$_3$-3 under under UV light (**c**) or visible light irradiation (**d**).

The photocurrents density of photocatalyst can further auxiliarily illustrate the separation and transfer of photo-generated electrons and holes[34]. As displayed in Fig. 7c, the photocurrents densities of pure AgIO$_3$ and the AgCl/AgI/AgIO$_3$ were investigated under visible light irradiation and all of them were reversible and stable when the light on or light off. The photocurrents density of AgCl/AgI/AgIO$_3$ composites firstly increased gradually and then decreased with the increase of HONH$_3$Cl. Additionally, the AgCl/AgI/AgIO$_3$-3 composite possesses the highest photocurrents density, reflecting its optimal photocatalytic activity, which is consistent with the PL analysis.

The electrochemical impedance spectroscopy (EIS) responses of the samples were also used to monitor the charge migration process on the electrodes, as presented in Fig. 7d. Customarily, the smallest arc radius on the EIS Nyquist plot indicated efficient separation of the photogenerated electrons and holes[35]. The arc radius of AgCl/AgI/AgIO$_3$-3 is smaller than that of pure AgIO$_3$ and other AgCl/AgI/AgIO$_3$, suggesting the improved transfer efficiency of photogenerated carriers in AgCl/AgI/AgIO$_3$-3 composites. On the basis of the above analysis, the visible light absorption properties, the separation and transfer of photo-generated electrons and holes can be effectively enhanced by the formation of AgCl/AgI/AgIO$_3$ composites, thus achieving superior photocatalytic performance.

To distinguish the role of active radicals on the photocatalytic degradation of MO over AgCl/AgI/AgIO$_3$-3 based on different light source, the trapping experiment was conducted. As revealed in Fig. 8a and b, ethylene diamine tetraacetic acid disodium salt (EDTA-2Na), benzoquinone (BQ) and tertiary butanol (TBA) were selected as scavengers for h$^+$, •O^{2-} and •OH, respectively. When the EDTA-2Na was added, the photocatalytic performance of AgCl/AgI/AgIO$_3$-3 under both UV light and visible light was inhibited greatly, which illustrated that h$^+$ was the primary active species. The photocatalytic oxidation ability of AgCl/AgI/AgIO$_3$-3 was also restrained by the addition of BQ, indicating that •O^{2-} played an auxiliary role on the photocatalytic degradation of MO over AgCl/AgI/AgIO$_3$-3 under different light source. The apparent rate constant k didn't change after the TBA added, which suggested that •OH was not affecting the photocatalytic performance of AgCl/AgI/AgIO$_3$-3.

Based on the abovementioned experimental results, the possible photocatalytic mechanism process was proposed in Fig. 8. When the photocatalysis reaction system with AgCl/AgI/AgIO$_3$-3 exposed to UV light (Fig. 8c), AgCl, AgI and AgIO$_3$ all can be activated by UV light photons and accompany electrons jumping from the valence band (VB) to the conduction band (CB). As depicted in Supplementary Table S1, the calculated CB energy levels of AgIO$_3$ is 0.26 eV, which is more positive than the CB potentials of AgI (−0.42 eV) and AgCl (−0.06 eV). Therefore, the photoinduced electrons of AgI and AgCl would migrate to the CB of AgIO$_3$. However, the CB potentials of AgIO$_3$ is excessively positive contrast to O$_2$/•O^{2-} (−0.046 eV vs. NHE), therefore it cannot reduce O$_2$ to produce •O^{2-}. While the •O^{2-} radicals have been detected during the trapping experiments, suggesting the Fermi energy of the AgIO$_3$ would move more negative position in the photocatalytic system to match well with the energy level of its surrounding medium[18,36]. Meanwhile, the whole energy level of the AgIO$_3$ rearranged and the conduction band of the AgIO$_3$ became more negative. Hence, it is possible to reduce O$_2$ to produce •O^{2-} by

the photoinduced electrons on the CB of $AgIO_3$ in this photooxidative process. At the same time, the photogenerated h^+ was remained and accumulated on the VB of AgI (2.37 eV) because that it is more negative than the VB of $AgIO_3$ (4.01 eV) and AgCl (3.19 eV), which could not oxidize -OH into •OH with the oxidative potential of 2.6 V vs. NHE[37,38]. The above mentioned results are in accordance with the trapping experiment. While under the irradiation of visible light (Fig. 8d), only AgI can be excited because of the native narrow band gap ($E_g = 2.8$ eV). The photogenerated electrons will transfer from AgI to $AgIO_3$ and reduce O_2 to produce •O^{2-}, meanwhile the photogenerated holes which remained on the VB of AgI will oxidize MO directly owing to its strong oxidative capacities. Consequently, no matter what the excitation light source used, the separation of photogenerated electron-hole pairs could be significantly improved because of the synergistic effect among the ternary materials. Besides, the conversion of a part of I^{5+} to I^- during the photocatalytic process may also have effects on the oxidation of dyes[39], as seen in Supplementary Fig. S7. Meanwhile, the generated silver atomic clusters during photocatalytic process can absorb visible light and thus induce the appearance of photogenerate electrons and holes, which is also benefit for enhancing the visible light photocatalytic performance of composite materials (Supplementary Fig. S8).

Conclusion

In conclusion, the novel $AgCl/AgI/AgIO_3$ composites were designed and synthesized by a facile and rapid one-pot *in situ* solid-state chemical technique. The $AgCl/AgI/AgIO_3$ composites displayed greatly upgraded photocatalytic performance for the degradation of MO under both UV light and visible light irradiation compared with pure $AgIO_3$, AgCl, AgI, and $AgI/AgIO_3$, which mainly depends on the enhanced light adsorption in full spectrum and the efficient charge separation on the surface. The efficient charge separation of the $AgCl/AgI/AgIO_3$ composites is attributed to the photogenerated electrons of AgI or AgCl could eventually transfer to the CB of $AgIO_3$, the holes would migrate to the VB of AgI simultaneously. This work may offer a simple avenue to realize rationally design of Ag-based heterojunction structures with tunable photocatatlytic performance.

Experiment

Preparation of $AgCl/AgI/AgIO_3$ composites. Every chemical used in this article is of analytical pure and used without further purification. The $AgCl/AgI/AgIO_3$ composites were synthesized by a room-temperature one-pot *in situ* solid-state reducing reaction. Firstly, 5 mmol of $AgNO_3$ was weighted and grinded into fine powder, then 5 mmol of KIO_3 was added and grinded for about 10 min, finally, a certain amount of $HONH_3Cl$ was added into the above mixture and ground for 30 min to ensure the completeness of the reaction. After reaction, the precipitate of the samples was collected and washed thoroughly with distilled water and absolute ethanol, and dried at room temperature in air for 1 h. The as-prepared composites with the amount of $HONH_3Cl$ of 1 mmol, 2 mmol, 3 mmol and 4 mmol are marked as $AgCl/AgI/AgIO_3$-1, $AgCl/AgI/AgIO_3$-2, $AgCl/AgI/AgIO_3$-3 and $AgCl/AgI/AgIO_3$-4, respectively.

The preparation process of $AgIO_3$ was the same as the preparation of $AgCl/AgI/AgIO_3$ composites except for the absence of $HONH_3Cl$.

Characterization. X-ray diffraction (XRD) was served to analyze the crystalline phase by a Bruker D8 using filtered Cu Kα radiation (1.54056 Å) with an operating voltage of 40 kV and a beam current of 40 mA. Energy dispersive X-ray spectrometer (EDX) and mapping was obtained on an Oxford 2000 with the accelerating voltage of 200 kV. Raman spectrum was measured using a Bruker spectrometer with a solid-state laser (excitation at 532 nm, 10 mW) at room temperature in the range of 1000-40 cm^{-1}. The X-Ray Photoelectron Spectroscopy (XPS) (ESCALAB 250Xi, Thermo Fisher Scientific, USA) was applied to investigate the chemical composition and the chemical states employing Al Kα 1486.6 eV. Field emission scanning electronic microscopy (FESEM, Hitachi, SU8010 at 5 kV) was performed to obtain the morphology of the samples. Transmission electron microscope (TEM) was acquired on a JEM-2100F at 200 kV (JEOL, Japan). The UV-vis diffuse reflectance spectroscopy was conducted on Hitachi U-3900H Spectrophotometer, using $BaSO_4$ as the reference, which was employed to measure the intrinsic absorption wavelength of the catalyst. Photoluminescence (PL) spectra of the as-prepared samples were measured on a fluorescence spectrophotometer (F-4500, Hitachi, Japan). The UV-Vis absorption spectrum was conducted on Hitachi U-3010 Spectrophotometer, which was used to analysis the absorption spectra of the degraded dyes. The photocatalytic experiments were carried out in an XPA-1 photochemical reactor (Xujiang Electromechanical Plant, Nanjing, China).

Photocatalytic activity test. The photocatalytic activity of the as-prepared samples were systematically evaluated by the degradation of MO under UV light (300 W Hg lamp, 6.06 mW/cm^2) illumination for 12 min or visible light (350 W Xe lamp with a ≥420 nm cutoff optical filter, 1.9 mW/cm^2) irradiation for 50 min, respectively. Both of the two lamps have been bought with XPA-1 photochemical reactor (Xujiang Electromechanical Plant, Nanjing, China). 25 mg of $AgCl/AgI/AgIO_3$ powders was ultrasonically dispersed in 50 ml MO solution (10 mg/L for UV light, 5 mg/L for visible light). Prior to illumination, the suspension was magnetically stirred in the dark for 0.5 h to reach the adsorption-desorption equilibrium between MO and the catalysts. During the whole process including adsorption in dark and UV light irradiation, 3 mL of the suspension was collected and centrifuged to remove the photocatalyst particles, and then analyzed by recording the UV-vis spectrum of MO at 463 nm within a given time intervals. The rhdamine B (RhB, 5 mg/L), methylene blue (MB, 5 mg/L), phenol (10 mg/L), bisphenol A (BPA, 10 mg/L) and tetracycline hydrochloride (10 mg/L) were also employed to evaluate the photocatalytic activity of the $AgCl/AgI/AgIO_3$-3 composite. Besides, the wavelength dependent photocatalytic activity over the $AgCl/AgI/AgIO_3$-3 composite was evaluated by the 300 W Xe lamp with different band-pass filter (CEL-SPH2N, Beijing, China), the corresponding optical power intensity was displayed in Supplementary Fig. S6.

Photoelectrochemical measurements. An electrochemical analyzer (CHI 660E) with a standard three electrode configuration was served to measure the photocurrents and electrochemical impedance spectroscopy (EIS) of the samples at room temperature. The photocurrent intensity was measured under intermittent illumination with a 300 W Xe lamp at 0.3 V. 0.5 mol·L^{-1} Na$_2$SO$_4$ aqueous solution was used as the electrolyte, the saturated Ag/AgCl electrode served as reference electrode, the Pt wire employed as counter electrode and the as-prepared samples coated on F-doped SnO$_2$-coated glass (FTO glass) substrate used as working electrode (photoanode). To fabricate the photoanode, 5 mg the as-prepared powder was ultrasonic disperse in 1 ml ethanol homogeneously, then the mixture were spread on an F-doped SnO$_2$-coated glass (FTO) substrate (1.0 cm × 2.0 cm), finally dried at 100 °C in an oven.

References

1. Osterloh, F. E. Inorganic Materials as Catalysts for Photochemical Splitting of Water. *Chem. Mater.* **20**, 35–54 (2008).
2. Tong, H. *et al*. Nano-photocatalytic materials: possibilities and challenges. *Adv. Mater.* **24**, 229–251 (2012).
3. Chen, X. B. & Mao, S. S. Titanium Dioxide Nanomaterials: Synthesis, Properties, Modifications, and Applications. *Chem. Rev.* **107**, 2891–2959 (2007).
4. Scuderi, V. *et al*. Rapid synthesis of photoactive hydrogenated TiO$_2$ nanoplumes. *Appl. Catal. B-Environ.* **183**, 328–3345 (2016).
5. Scuderi, V. *et al*. TiO$_2$-coated nanostructures for dye photo-degradation in water. *Nanoscale Res. Lett.* **9**, 1–7 (2014).
6. Hernandez-Alonso, M. D., Fresno, F., Suarez, S. & Coronado, J. M. Development of alternative photocatalysts to TiO$_2$: challenges and opportunities. *Energy Environ. Sci.* **2**, 1231–1257 (2009).
7. Aguirre, M. E., Zhou, R., Eugene, A. J., Guzman, M. I. & Grela, M. A. Cu$_2$O/TiO$_2$ heterostructures for CO$_2$ reduction through a direct Z-scheme: Protecting Cu$_2$O from photocorrosion. *Appl. Catal. B-Environ.* **217**, 485–493 (2017).
8. He, C. N. *et al*. Tuning near-gap electronic structure, interface charge transfer and visible light response of hybrid doped graphene and Ag$_3$PO$_4$ composite: Dopant effects. *Scientific Reports* **6**, 22267 (2016).
9. Jing, L. Q. *et al*. Novel magnetic CoFe$_2$O$_4$/Ag/Ag$_3$VO$_4$ composites: highly efficient visible light photocatalytic and antibacterial activity. *Appl. Catal. B-Environ.* **199**, 11–22 (2016).
10. Lin, Z. Y. *et al*. Electronic reconstruction of α-Ag$_2$WO$_4$ nanorods for visible-light photocatalysis. *ACS Nano* **9**, 7256–7265 (2015).
11. Dai, G. P., Yu, J. G. & Liu, G. A new approach for photocorrosion inhibition of Ag$_2$CO$_3$ photocatalyst with highly visible-light-responsive reactivity. *J. Phys. Chem. C* **116**, 15519–15524 (2012).
12. Huang, H. W. *et al*. Hydrothermal synthesis, nonlinear optical property and photocatalytic activity of a non-centrosymmetric AgIO$_3$ photocatalyst under UV and visible light irradiation. *Solid State Sci.* **46**, 37–42 (2015).
13. Cao, Q. W., Zheng, Y. F. & Song, X. C. Enhanced visible-light-driven photocatalytic degradation of RhB by AgIO$_3$/WO$_3$ composites. *J. Taiwan Inst. Chem. E.* **000**, 1–7 (2016).
14. Cao, Q. W., Zheng, Y. F., Yin, H. Y. & Song, X. C. A novel AgI/AgIO$_3$ heterojunction with enhanced photocatalytic activity for organic dye removal. *J. Mater. Sci.* **51**, 4559–4565 (2016).
15. Zeng, C. *et al*. Facile *in-situ* self-sacrifice approach to ternary hierarchical architecture Ag/AgX(X = Cl, Br, I)/AgIO$_3$ distinctively promoting visible-light photocatalysis with composition-dependent mechanism. *ACS Sustainable Chem. Eng.* **4**, 3305–3315 (2016).
16. Li, Y. F. *et al*. Ultrathin g-C$_3$N$_4$ nanosheets coupled with AgIO$_3$ as highly efficient heterostructured photocatalysts for enhanced visible-light photocatalytic activity. *Chem. Eur. J.* **21**, 17739–17747 (2015).
17. He, Z. Q., Wang, D., Fang, H. Y., Chen, J. M. & Song, S. Highly efficient and stable Ag/AgIO$_3$ particles for photocatalytic reduction of CO$_2$ under visible light. *Nanoscale* **6**, 10540–10544 (2014).
18. Zeng, C. *et al*. Dual redox couples Ag/Ag$^+$ and I$^-$/(IO$_3$)$^-$ self-sacrificed transformation for realizing multiplex hierarchical architectures with universally powerful photocatalytic performance. *Appl. Catal. B-Environ.* **200**, 620–632 (2017).
19. Wang, R. Y. *et al*. Rapid synthesis of amino acid polyoxometalate nanotubes by one-step solid-state chemical reaction at room temperature. *Adv. Funct. Mater.* **16**, 687–692 (2006).
20. Ye, X. R., Jia, D. Z., Yu, J. Q., Xin, X. Q. & Xue, Z. L. One-step solid-state reactions at ambient temperatures-a novel approach to nanocrystal synthesis. *Adv. Mater.* **11**, 941–942 (1999).
21. Hu, P. F., Cao, Y. L., Jia, D. Z., Li, Q. & Liu, R. L. Engineering the metathesis and oxidation-reduction reaction in solid state at room temperature for nanosynthesis. *Scientific Reports* **4**, 4153 (2014).
22. Kang, S. F. *et al*. Critical influence of g-C$_3$N$_4$ self-assembly coating on the photocatalytic activity and stability of Ag/AgCl microspheres under visible light. *Appl. Catal. B-Environ.* **168–169**, 472–482 (2015).
23. Belkhair, S. *et al*. Silver zeolite-loaded silicone elastomers: a multidisciplinary approach to synthesis and antimicrobial assessment. *RSC Adv.* **5**, 40932–40939 (2015).
24. Dong, F. *et al*. Facets and defects cooperatively promote visible light plasmonic photocatalysis with Bi nanowires@BiOCl nanosheets. *J. Catal.* **344**, 401–410 (2016).
25. Yang, S. B. *et al*. *In-situ* synthesis of a plasmonic Ag/AgCl/Ag$_2$O heterostructures for degradation of ciprofloxacin. *Appl. Catal. B-Environ.* **204**, 602–610 (2017).
26. Meng, X. C. & Zhang, Z. S. Plasmonic ternary Ag-rGO-Bi$_2$MoO$_6$ composites with enhanced visible light-driven photocatalytic activity. *J. Catal.* **344**, 616–630 (2016).
27. Yan, R. Y. *et al*. Bio-inspired plasmonic nanoarchitectured hybrid system towards enhanced far red-to-near infrared solar photocatalysis. *Scientific Reports* **6**, 20001 (2016).
28. Wei, N. *et al*. Ag$_2$O nanoparticle/TiO$_2$ nanobelt heterostructures with remarkable photo-response and photocatalytic properties under UV, visible and near-infrared irradiation. *Appl. Catal. B-Environ.* **198**, 83–90 (2016).
29. Zhou, R. X. & Guzman, M. I. Photocatalytic reduction of fumarate to succinate on ZnS mineral surfaces. *J. Phys. Chem. C* **120**, 7349–7357 (2016).
30. Zhou, R. X. & Guzman, M. I. CO$_2$ Reduction under periodic illumination of ZnS. *J. Phys. Chem. C* **118**, 11649–11656 (2014).
31. Li, H. J., Zhou, Y., Tu, W. G., Ye, J. H. & Zou, Z. G. State-of-the-Art progress in diverse heterostructured photocatalysts toward promoting photocatalytic performance. *Adv. Funct. Mater.* **25**, 998–1013 (2015).
32. Xu, D. B. *et al*. *In-situ* synthesis and enhanced photocatalytic activity of visible-light-driven plasmonic Ag/AgCl/NaTaO$_3$ nanocubes photocatalysts. *Appl. Catal. B-Environ.* **191**, 228–234 (2016).
33. Huang, H. W. *et al*. Anionic group self-doping as a promising strategy: band-gap engineering and multi-functional applications of high-performance CO$_3$$^{2-}$ doped Bi$_2$O$_2$CO$_3$. *ACS Catal.* **5**, 4094–4103 (2015).
34. Lv, Y. H., Yao, W. Q., Zong, R. L. & Zhu, Y. F. Fabrication of wide-range-visible photocatalyst Bi$_2$WO$_{6-x}$ nanoplates via surface oxygen vacancies. *Scientific Reports* **6**, 19347 (2016).
35. Su, T. M., Tian, H., Qin, Z. Z. & Ji, H. B. Preparation and characterization of Cu modified BiYO$_3$ for carbon dioxide reduction to formic acid. *Appl. Catal. B-Environ.* **202**, 364–373 (2017).
36. Ye, L. Q. *et al*. Two different roles of metallic Ag on Ag/AgX/BiOX (X = Cl, Br) visible light photocatalysts: surface plasmon resonance and Z-scheme bridge. *ACS Catal.* **2**, 1677–1683 (2012).
37. Huang, Y. *et al*. *In situ* fabrication of α-Bi$_2$O$_3$/(BiO)$_2$CO$_3$ nanoplate heterojunctions with tunable optical property and photocatalytic activity. *Scientific Reports* **6**, 23435 (2016).

38. Wang, J. C. *et al*. Enhanced photoreduction CO_2 activity over direct Z-scheme α-Fe_2O_3/Cu_2O heterostructures under visible light irradiation. *ACS Appl. Mater. Inter.* **7**, 8631–8639 (2015).
39. Pillar, E. A., Guzman, M. I. & Rodriguez, J. M. Conversion of iodide to hypoiodous acid and iodine in aqueous microdroplets exposed to ozone. *Environ. Sci. Technol.* **47**, 10971–10979 (2013).

Author Contributions

J.X. prepared and characterized the materials, and performed photocatalytic activity testing, C.Y.L., D.Z.J. and Y.Z.L. commented on the manuscript writing and the result discussion, K.W. and H.X. helped to complete part of the characterization and testing. All authors reviewed the manuscript.

Additional Information

Supplementary information accompanies this paper at https://doi.org/10.1038/s41598-017-12625-8.

Competing Interests: The authors declare that they have no competing interests.

Publisher's note: Springer Nature remains neutral with regard to jurisdictional claims in published maps and institutional affiliations.